# FINAL REPORT

## MINOR RESEARCH PROJECT :

## INVESTIGATIONS ON ELECTRICAL, MAGNETIC, ELECTROCHEMICAL BEHAVIOUR OF NASICON AND OLIVINE MATERIALS

(UGC letter No. F. MRP(S)-0793/13-14/KLMG019/UGC-SWRO dated 28.03.2014)

**PRINCIPAL INVESTIGATOR: DR. LAKSHMI VIJAYAN**

**ASSISTANT PROFESSOR**

**DEPARTMENT OF PHYSICS**

**ST. ALOYSIUS COLLEGE**

**EDATHUA**

**ALZPPUZHA (DIST)**

**KERALA**

**(i) The objectives of the present project are:**

(a) The NASICON and OLIVINE type materials are planned to synthesize in nanocrystalline form by hydrothermal technique.

(b) The existing power laws namely: Jonscher's power law, Cole-Cole, Cole-Davidson, Havriliak-Negami frequency domain dielectric function and time domain Williams-Watts were planned to use for the analysis of the electrical data.

(c) Application of these matreials in Li ion battery is also planned-Electrochemical study

**(ii) Work done so far and results achieved and publications, if any, resulting from the work:**

A series of lithium transition metal phosphates with an ordered Olivine structure $LiMPO_4$ (M = Fe, Mn, Co, Ni) have recently been investigated as attractive cathode materials because of their non-toxic, environment friendly and excellent thermal stability. Therefore, many research groups have focused their efforts on new synthesis methods for the preparation of Olivine phosphates specially lithium manganese phosphate to improve their performances.

The synthesis of inorganic nanocrystals has attracted considerable interest due to dramatic improvements caused by nano-effect. Olivine $LiMnPO_4$ is now recognized as a promising cathode material for lithium ion batteries with potential application because of low cost, environmentally benign constituents and high theoretical capacity.

Compared with the popular $LiFePO_4$ cathode material, $LiMnPO_4$ is of particular interest to the battery community because of the ideal location of the $Mn^{2+}/Mn^{3+}$ couple at 4.1 V vs. $Li/Li^+$, which is 0.65V higher than $LiFePO_4$, and its theoretical energy density (684Wh/kg = 171mAh/g × 4.0V) is 1.2 times larger than that of $LiFePO_4$ (578Wh/kg = 170mAh/g × 3.4V). The main drawback of $LiMnPO_4$ is their low electronic conductivity, which results in poor rate capability. Since Li et al. first reported the reversible reaction of Mn (II) ↔Mn (III) in olivine phosphate, researchers have tried various methods to prepare electro-active $LiMnPO_4$ to overcome the limitation on its application.

Developing specific synthesis methods appropriating for designing $LiMnPO_4$ in the nano-scale region is in great need to improve the kinetics of $LiMnPO_4$, as it has been proved that decreasing the size of the crystallites to nano-scale offers potential for higher electrode/electrolyte surface contact, less mechanical strain upon lithium intercalation from the

lattice than the bulk materials and reduces path length for lithium-ion/electron transport through the material.

Critical to the success of new cathode materials, is their preparation, which controls the morphology, particle size and cation order amongst other critical parameters. Although traditionally high-temperature methods have been used, they are both energy intensive and cannot readily produce many potentially metastable structures that might result in high lithium ion diffusivity. However, they do have the advantage of being hydroxyl/water free. There are many possible approaches to the synthesis of active materials, but in the end a commercially viable approach must be used [1]. Soft chemical approaches, such as hydrothermal/solvothermal or ion exchange offer several advantages. Such methods are used on the tonnage quantities today, and so the chemical industry considers them viable. Hydrothermal synthesis has been extensively studied for simple oxides such as those of tungsten, molybdenum and vanadium, and today many of the key parameters are understood [2,3]. Various phosphates have also been successfully prepared.

A cathode of particular interest is lithium iron phosphate, LiMnPO4, with the olivine structure [4]. This material is conventionally synthesized at elevated temperatures, but to take advantage of its low cost components it would be advantageous to use a low cost, low energy utilization synthesis approach.

Hydrothermal method is used for the synthesis of $LiMnPO_4$. Hydrothermal synthesis can be defined as a method of synthesis that depends on the solubility of minerals in hot water under high pressure. $LiMnPO_4$ is prepared from $LiNO_3$, Mn $(NO_3)_2$. $4H_2O$ and $NH_4H_2PO_4$. Reaction is carried out in a sucrose medium which acts as template. Metal precursor is dissolved in distilled water keeping the sucrose to metal molar ratio at 2:1, 4:1, 6:1, 8:1 and 10:1. During the hydrothermal treatment, carbon sphere are formed with metal ions incorporated in hydrophilic shell. The removal of carbon through calcinations yields $LiMnPO_4$.

## CRYSTAL STRUCTURE

A crystal structure is a unique arrangement of atoms or molecules in a crystalline liquid or solid. A crystal structure describes highly ordered structure, occurring due to intrinsic nature of molecules to form symmetric patterns. A crystal structure can be an infinitely repeating array of 3D unit cells. The unit cell is calculated from the simplest possible representation of molecules, known as the symmetric unit.

The asymmetric unit is translated to unit cell through symmetric operations, and the resultant crystal lattice is constructed through repetition of the unit cell infinitely in 3-

dimensions. Patterns are located upon the points of a lattice, which is an array of points repeating periodically in three dimensions. The lengths of edges of a unit cell and the angles between them are called the lattice parameters. The symmetry properties of the crystal are embodied in its space group. A crystal structure and symmetry play a role in determining many of its physical properties, such as cleavage, electronic band structure and optical transparency.

The defining property of a crystal is its inherent symmetry, by which we mean that under certain 'operations' the crystal remain unchanged. All crystals have translational symmetry in three directions, but some have other symmetry element as well. For example, rotating the crystal $180^0$ about a certain axis may result in an atomic configuration that is identical to the original configuration. The crystal is then said to have a two-fold rotational symmetry about this axis. In addition to rotational symmetries like this, a crystal may have symmetries in the form of mirror planes and translational symmetries, and also so-called compound symmetries, which are a combination of translation and rotation/mirror symmetries.

Lattice systems are grouping of crystal structures according to the axial system used to describe their lattice. Each lattice system consists of a set of three axes in a particular geometric arrangement. There are seven lattice systems. They are cubic, hexagonal, tetragonal, rhombohedral, orthorhombic, monoclinic and triclinic.

**POINT GROUP:**

The crystallographic point group is the mathematical group comprising the symmetry operations that leave at least one point unmoved and that leave the appearance of the crystal structure unchanged. These symmetry operations include

- Reflection, which reflects the structure across a reflection plane.
- Rotation, which rotates the structure a specified portion of a circle about a rotation axis.
- Inversion, which changes the sign of the coordinate of each point with respect to a centre of symmetry or inversion point.
- Improper rotation, which consists of a rotation about an axis followed by an inversion.

Rotation axes (proper and improper), reflection planes and centre of symmetry are collectively called symmetry elements. There are 32 possible crystal classes.

**SPACE GROUP:**

The space group of the crystal structure contains translational symmetric operations, these include:

- Pure translations, which move a point along a vector.
- Screw axes, which rotate a point around an axis while translating parallel to the axis.
- Glide planes, which reflect a point through a plane while translating it parallel to the plane.

## OLIVINE STRUCTURE

Lithium manganese phosphate ($LiMnPO_4$) has an olivine structure, where Mn and Li occupy octahedral 4c and 4a sites, and P atom is in 4c site, respectively. The O atoms are in a hexagonal close-packed arrangement. The $MnO_6$ octahedral is separated by $PO_4$ plain that leads to the significant reduction of the electrical conductivity of the material. It results in a poor rate capability and a slow utilization of Li ions in the olivine host structure. Therefore, the successful preparation of high performance $LiMnPO_4$ could be achieved through the preparation of the conductive composites of fine particles of this material.

In the olivine structures the magnetic ions occupy only the so-called $M_2$ site, *i.e.* the $M^{2+}$ ion sits in the center of $MO_6$ unit. Each $MO_6$ distorted octahedron is connected to four other $MO_6$ via vertices forming a layered network perpendicular to the crystal (100) direction. Successive $M^{2+}$ layers are separated by $PO_4$ tetrahedral and $LiO_6$ octahedral.

Olivine-type LiMnPO4 compounds have an orthorhombic structure comprised of close-packed phosphate anions with $Mn^{2+}$ ions in corner sharing $MO_6$ sites and Li ions in edge sharing $LiO_6$ sites. The strong P–O covalent bond gives these materials good stability and makes them attractive as positive electrodes for lithium batteries in vehicle applications [5]. $LiMnPO_4$ (lithiophilite) cycles at a nearly constant potential of 4.1 V vs. $Li/Li^+$, which is well suited to use in standard battery configurations [5]. In contrast with $LiFePO_4$, however, the manganese compound suffers from poor Li extraction and insertion kinetics. Many factors have been considered to contribute to the slow phase transition, including the electronic and ionic conductivities, the Jahn Teller effect in $Mn^{3+}$, interface strain due to the large volume change between $LiMnPO_4$ and $MnPO_4$, and the metastable nature of the delithiated phase. Although the mechanism of the two-phase reaction has not been identified, it is likely that it is similar to that of the $LiFePO_4/FePO_4$ system. Previous efforts to improve the performance of stoichiometric $LiMnPO_4$ have mostly been limited to particle size minimization, which increases the rate and utilization, but inevitably decreases the volumetric energy density of the electrode. [5]

Fig 1: Structure of $LiMnPO_4$ Fig 2: Structure of $LiMnPO_4$

As mentioned before, critical success of cathode materials is in their preparation, which controls the morphology, particle size and cation order amongst other critical parameters [6]. Although traditionally high temperature methods have been used, they are both energy intensive and cannot readily produce many potentially metastable structures that might result in high lithium ion diffusivity [6]. However, they do have the advantage of being hydroxyl/water free. There are many possible approaches to the synthesis of active materials, but in the end a commercially viable approach must be used. Soft chemical ap-proaches, such as hydrothermal/solvothermal or ion exchange offer several advantages. Such methods are used on the tonnage quantities today, and so the chemical industry considers them viable. Hydrothermal synthesis has been extensively studied for simple oxides such as those of tungsten, molybdenum and vanadium, and today many of the key parameters are understood. Various phosphates have also been successfully prepared [6]. Hence, our experimental procedure will also follow the hydrothermal synthesis of the $LiMnPO_4$ cathodes.

## REFERRANCES


[1] M.S. Whittingham, in: G.-A. Nazri, G. Pistoia (Eds.), Lithium Batteries, Kluwer Academic Publishers, Boston, 2004, p. 85.

[2] T.A. Chirayil, P.Y. Zavalij, M.S. Whittingham, Chem. Commun. (1997) 33.

[3] T.A. Chirayil, P.Y. Zavalij, M.S. Whittingham, Chem. Mater. 10 (1998) 2629.

[4] A.K. Padhi, K.S. Nanjundaswamy, J.B. Goodenough, J. Electrochem. Soc. 144 (1997) 1188

[5] Z Bakenov and I Taniguchi, Open Materials Science Journal, vol. 5 (2011) 227.

[6] J Chen, M.J Vacchio, S Wang, N Chernova, P.Y Zavali and M.S Whittingham. Solid State Ionics, Vol. 178 (2008) 1676.

# SYNTHESIS AND CHARACTERIZATION TECHNIQUES

This chapter describes the synthesis and characterization techniques explored in the present study. Different methods are available for the synthesis of $LiMnPO_4$ like,

- sol gel method
- solution combustion
- solid state synthesis
- hydrothermal method

In the present study, $LiMnPO_4$ is synthesized using hydrothermal method. Reaction is carried out in a sucrose medium which acts as template. Metal precursor is dissolved in distilled water keeping the sucrose to metal molar ratio at 2:1, 4:1, 6:1, 8:1, 10:1. The synthesised sample is characterized using X-Ray diffraction**.**

## 2.1 SOL GEL METHOD

In sol-gel method "formation of an oxide network is through polycondensation reactions of a molecular precursor in a liquid". A sol is a stable dispersion of colloidal particles or polymers in a solvent. The particles may be amorphous or crystalline. An aerosol is particles in a gas phase, while sol is particles in a liquid. A gel consists of a three dimensional continuous network, which encloses a liquid phase, in a colloidal gel, the network is built from agglomeration of colloidal particles.

The idea behind sol-gel synthesis is

- To "dissolve" the compound in a liquid in order to bring it back as a solid in a controlled manner.
- Multi component compounds may be prepared with a controlled stoichiometry by mixing sols of different compounds.
- The sol-gel method prevents the problems with co-precipitation, which may be inhomogeneous, be a gelation reaction.
- Enables mixing at an atomic level.
- Results in small particles, which are easily sinterable.

## 2.2 SOLUTION COMBUSTION

Solution combustion is an effective method for synthesis of nano-size materials and it has been used for the production of a variety of fine complex oxide powders for different advanced applications, including catalysts, fuel cells and biotechnology. However, it is surprising that

while essentially all of the studies on it emphasize the characterization of the synthesized materials, little information is available on controlling combustion parameters and the reaction mechanism.

Combustion synthesis has emerged as a facile and economically viable technique for the preparation of advanced ceramics, catalysts and nonmetal. Recent innovations in the combustion and processing parameters have resulted in a better understanding of combustion phenomena and control of microstructure and property of the products. Based on the fundamental understanding of the considered combustion processes, a variety of extremely high surface area materials could be synthesized.

## 2.3 SOLID STATE SYNTHESIS

Solid state synthesis of heating two non-volatile solids which react to form the required product and this method can be used to prepare an extremely large number of compounds and this can be also used to prepare a whole range of materials including mixed metal oxides, sulfides, nitrites, aluminosilicates etc. The term solid-state synthesis is often used to describe interactions where neither a solvent medium nor controlled vapor phase interactions are utilized. Solid-state synthesis is used to create the unique compositions and morphologies needed to generate the described attributes in scintillation crystals, piezoelectric and other advanced materials.

Criteria for the solid state synthesis of large, nearly defect free, polymer crystals are derived and related to experimental observations. The trend in modern solid-state synthesis resembles approach used in small-molecule chemistry, in the sense that attention to reaction mechanism and the use of molecular building blocks result in an ability to prepare new materials of designed structure. Advantages of solid states are simplicity, lower reaction temperatures possibly stabilize metastable phases, eliminate intermediate impurity phases and the disadvantages of solid states are high temperature are generally required .The desired compound may decompose at high temperatures. The reaction may proceed very slowly, but increasing the temperature speed up the reaction since it increases the diffusion rate.

## 2.4 HYDROTHERMAL SYNTHESIS

Hydrothermal synthesis can be defined as a method of synthesis that depends on the solubility of minerals in hot water under high pressure. Hydrothermal synthesis includes the various techniques of crystallizing substances from high-temperature aqueous solution at high vapor pressures. It is performed in an apparatus consisting of a steel pressure vessel called an autoclave, in which a nutrient is supplied along with water.

Hydrothermal process is a technique in which a heterogeneous reaction in the presence of aqueous solvents under high pressure and temperature conditions to dissolve and recrystallize materials that are relatively insoluble under ordinary conditions. Hydrothermal technique is ideal for processing of very fine powders having high purity, controlled stoichiometry, high quality, narrow particle size distribution, a controlled morphology, uniformity, less defects, dense particles, high crystallinity, excellent reproducibility, controlled microstructure, and high reactivity with ease of sintering and so on.

During the hydrothermal treatment, carbon sphere are formed with metalions incorporated thermohydrophilic shell. The removal of carbon via calcinations yields hollow metal oxide spheres. Using this procedure, we can produce,a wide range of metal oxide hollow sphere.

Owing to their low density, large specific surface area, hollow structure, and nanostructured wall, hollow spheres with nanometer or micrometer size often exhibit special physical and chemical properties different from solid particles. Hollow spheres have potential applications in many areas, such as optics, electrics, magnetics, medicine-release capsules, drug delivery, light-weight filler, selective adsorption, and atalysis.[1–4] Therefore, there has been great interest in preparing hollow structures with different compositions in recent years.

The hollow spheres with nanocrystalline or amorphous shells were prepared through a variety of routes, among which the template routes including hard template and soft template methods were frequently applied. In the hard template process, a coating is formed first on the template (core) by controlled surface precipitation, and then the core is removed by thermalor chemical means to form hollow spheres. A variety of colloid particles such as silica particles, polystyrene spheres, carbon spheres, an so on have been used as hard templates to fabricate hollow spheres.[1–5].

Fig. 3: Schematic illustration of the synthesis procedure used for obtaining the dense core–shell $SnO_2$/C spheres Jun Liu, Wen Li *et. al.*

Carbon spheres were often used as the template to synthesize hollow spheres. The process usually includes four steps:

(1) Preparation of the carbon spheres by hydrothermal carbonization
(2) Separation of the carbon spheres from the mixture
(3) Formation of the carbon/metal salt core–shell composite and
(4) Removal of the carbon cores to form the hollow spheres

Introducing a carbon core as a physical buffer is better than leaving an empty space to improve the cyclability. the carbon core can act as a buffer to prevent the collapse of $MnO_6$ shell caused by the large volume change occurring during the charge discharge process.

In here, $LiMnPO_4$ hollow sphere was prepared by hydrothermal treatment. First, the carbon spheres were formed by a hydrothermal process. Due to the abundant number of hydroxyl groups on the surface of the carbon spheres, the Li and $Mn^+$ cations could be adsorbed onto them, thus forming an amorphous composite shell rather than a crystalline coating from heterogeneous nucleation, which was confirmed by XRD analysis. In the subsequent calcination process, theadsorbed water and organics as well as the carbon core were removed, and the crystalline $LiMnPO_4$ is formed.

## 2.6 MERITS

Hydrothermal synthesis offers many advantages over conventional and non-conventional ceramic synthetic methods. All forms of ceramics can be prepared with hydrothermal synthesis namely powders, fibers and single crystals, monolithic ceramic bodies and coatings on metals, polymers and ceramics. From the standpoint of ceramic powder production, there are far fewer time- and energy-consuming processing steps since high temperature calcination, mixing, and milling steps are either not necessary or minimized. Moreover, the ability to precipitate already crystallized powders directly from solution regulates the rate and uniformity of nucleation,

growth and aging which results in improved control of size and morphology of crystallites and significantly reduced aggregation levels that is not possible with many other synthesis processes.

Fig 4: Schematic Illustration of the Synthesis of Metal Oxide Hollow Spheres from Hydrothermally Treated Carbohydrate/Metal Salt Mixtures.

The elimination or reduction of aggregates combined with narrow particle size distributions in the starting powders leads to optimized and reproducible properties of ceramics because of better microstructure control. Precise control of powder morphology can also be significant. For instance, powders with crystallites having well-developed shapes corresponding to particular crystallographic directions such as whiskers, plates, or cubes can be oriented to form materials with single crystal-like properties, such as polymer-ceramic composites or textured ceramic-ceramic composites with anisotropic properties.

Another important advantage of the hydrothermal synthesis is that the purity of hydrothermally synthesized powders significantly exceeds the purity of the starting materials. It is because the hydrothermal crystallization is a self-purifying process, during which the growing crystals/crystallites tend to reject impurities present in the growth environment. The impurities are subsequently removed from the system together with the crystallizing solution, which does not take place during other synthesis routes, such as high temperature calcination.

## CHARACTERISATION TECHNIQUES

### (1) X-RAY DIFFRACTION

X- ray diffraction is an important tool to determine the crystal structure of materials. X- rays are electromagnetic radiations having shorter wavelength (in the order of 0.1nm). X-rays can be diffracted by crystalline substances consisting of regularly arranged parallel rows of atoms separated by a distance called interplanar distance (in the order of few angstroms). When radiation enters a crystalline substance, X- rays get reflected by these parallel planes. The diffraction is the consequence of constructive interference of these reflected rays. The condition for such diffraction pattern was obtained from Bragg's law

$$2d\sin\theta = n\lambda$$

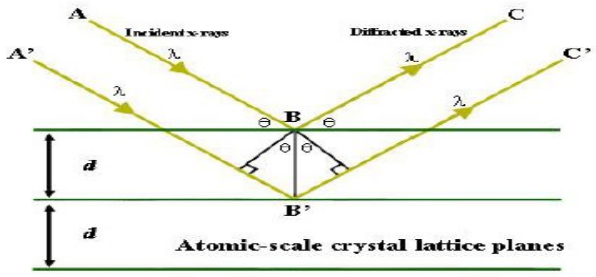


Fig 5: Schematic diagram of Bragg's diffraction

where θ is the angle of incidence, d is the distance between atomic layers in a crystal, λ is the wavelength of the incident X-ray beam and n is an integer, gives the order of diffraction. Constructive interference occurs only for certain values of θ correlating to a (hkl) plane, specifically when the path difference is equal to n times the wavelength. Fig (4) shows the schematic diagram explaining the Bragg's law. From Bragg's equation, the interplanar distance d, can be estimated using the other three known quantities

$$d = \frac{nl}{2\sin\theta}$$

The crystallite size can be calculated using the Scherrer's formula:

where, k is the constant dependent on crystallite shape, λ is the x-ray wavelength, β is the FWHM (full width at half maximum) and θ is the Bragg angle. X- ray diffraction data is used to determine the dimension of the unit cell.

# FOURIER TRANSFORM INFRARED SPECTROSCOPY

FTIR is a technique which is used to obtain an infrared spectrum of absorption or emission of a solid, liquid or gas. An FTIR spectrometer simultaneously collects high spectral resolution data over a wide spectral range. The resulting spectrum represents the molecular absorption and transmission, creating a molecular fingerprint of the sample. Like a fingerprint no two unique molecular structures produce the same infrared spectrum. This makes IR spectroscopy useful for several types of analysis. By FTIR, we can identify unknown materials, can be used to determine the quality or consistency of a sample, can determine the amount of components in a mixture etc.

The term FTIR originates from fact that a Fourier transform (a mathematical process) is required to convert the row data into the actual spectrum. It relies on the fact that the most molecules absorb light in the infrared region of the electromagnetic spectrum. This absorption corresponds specially to the bonds present in the molecule. The frequency range are measured as wavenumbers typically over the range 4000 – 600 $cm^{-1}$. The background emission spectrum of the IR source is first recorded, followed by the emission spectrum of the IR source with the sampling space. The ratio of the sample spectrum to the background spectrum is directly related to the sample's absorption spectrum. The resultant absorption spectrum from the bond natural vibration frequencies indicates the presence of various chemical bonds and functional groups present in the sample. FTIR is particularly useful for identification of organic molecular groups and compounds due to the range of functional groups, side chains and cross-links involved, all of which will have characteristics vibrational frequencies in the infrared range.

FTIR provide a wide range of information such as:

- It is a non-destructive technique

- It provides a precise measurement method which requires no external calibration
- It can increase the speed, collecting a scan every second
- It can identify unknown materials
- It can determine the quality or consistency of a sample and determine the amount of components in a mixture.

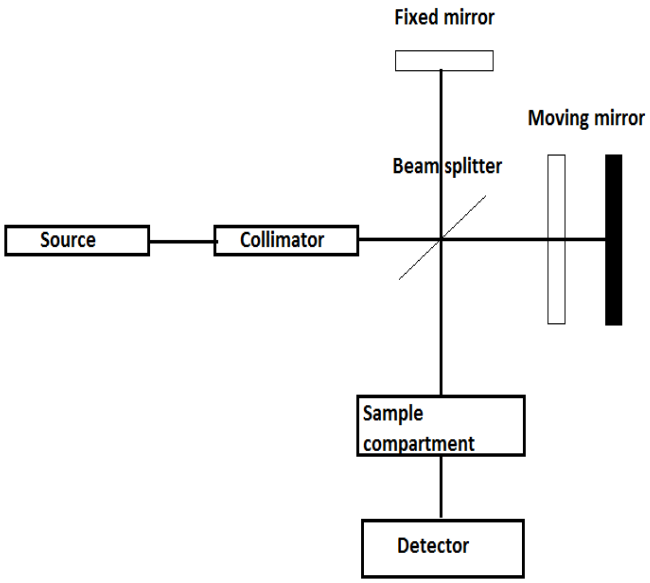


**Fig 2:** Schematic diagram of Fourier transform spectroscopy

The main difficulty was the slow scanning process for measuring all of the infrared frequency. Most infrared spectrometer splits the infrared beam into two optical beams. One beam reflects off a flat mirror which is fixed, other beam reflects off flat mirror which is the mechanism, which allows this mirror to move short distance (typically a few millimeters) away from the beam splitter. The two mirrors reflects off respective beams and are recombined when back at the beam splitter. Because the path that travels is a fixed length and the other is consistently changes as mirror moves with the signal. The interference is the result of these two beams interfering with each other. The result is fed to interferogram, which has the unique property that every data point which makes up the signal has information about every infrared which comes from the source.

In the interferogram, all the frequencies are being measured simultaneously and thus the use of the interferometer results in extremely fast measurements. The decoding of the individual measurements can be done using mathematical technique called Fourier transformation. This transformation is performed by the computer which then present the user with the desired spectral information.

The advantages of FTIR techniques have made significant impact with regard to

- rapid scanning
- signal to noise (S/N ) ratio
- high sensitivity
- high resolution
- data processing

**ELECTRICAL STUDY**

The impedance measurements of these samples are carried out in the temperature range of 373K-473K, since the dc resistance of olivine is high at low temperatures. The ac electrical measurements are carried out using broad band dielectric spectrometer in the frequency range of 50Hz to 1MHz. The present study uses complex impedance formalism for the extraction of ac electrical parameters at different temperatures. The elements of an equivalent circuit model represent various (macroscopic) processes involved in the transport of mass and charge. Using NLLS techniques, all the parameters in the equivalent circuit are adjusted simultaneously, thus obtaining the optimum fit to the measured dispersion data. A more general NLLS fit program based on the Marquardt algorithm has been used. The impedance parameters are obtained by fitting the data to an equivalent circuit using NLLS fitting procedure due to Boukamp.

## RESULTS AND DISCUSSION

### SYNTHESIS OF $LiMnPO_4$ USING HYDROTHERMAL METHOD

#### (1) Sucrose as template

Hydrothermal method is used for the synthesis of $LiMnPO_4$. $LiMnPO_4$ is prepared from $LiNO_3$, $Mn(NO_3)_2$. $4H_2O$ and $NH_4H_2PO_4$. Reaction is carried out in a sucrose medium

which acts as template. For the preparation of $LiMnPO_4$ in 2:1 moles, using sucrose as template, mole percentage of template is 2% and that of reactants is 1%.

Chemical reagents and sucrose where mixed in various molar ratios in double distilled water and stirred at room temperature. The solution transferred to 50 ml Teflon- limed stainless- steel autoclave was heat treated to $120^0$C for 20 hours; the products obtained were precipitated directly at the bottom of autoclave. The obtained sample is finely powdered and sintered for 6 hours at $700^0$C. The sample is grinded to fine powders. The above procedure is repeated for 4:1, 6:1, 8:1, 10:1 fuel ratios.

The chemical reaction is shown below:

$$7LiNO_3 + 7Mn(NO_3)_2.4H_2O + 7NH_4H_2PO_4 \rightarrow 7LiMnPO_4 + 4NH_3 + 43H_2O + 24NO_2$$

It is a very simple and scalable pathway towards metal oxide hollow spheres has been explored using hydrothermal synthesis. After the hydrothermal treatment of mixtures of carbohydrates with different metal salts in water in sealed steel autoclaves at 120°C, carbon spheres with the metal precursors tightly embedded in the microspheres were obtained. The removal of carbon directly results in $LiMnPO_4$ nanoparticles with high surface areas.

Fig 6: The images of experimental apparatus (a) autoclave (b) furnace (c) and (d) samples calcined at $120^0$C and $700^0$C.

## XRD ANALYSIS

The formation of $LiMnPO_4$ is confirmed by the XRD analysis.The XRD pattern of the samples analysed using Xpert high score software. The graphs are plotted using ORIGIN software. The grain size is calculated from the FWHM of the priminent peaks using Scherrer formula. The d spacing and lattice parameters are calculated using UNIT CELL software.

Table 1: Grain size of $LiMnPO_4$ (2:1) using Scherrer formula

| h | k | l | $2\theta$ (degree) | FWHM | Grain Size (nm) | Mean (nm) |
|---|---|---|---|---|---|---|
| 2 | 0 | 0 | 29.084 | .50724 | 161.8835 | 162.7287 |
| 1 | 3 | 1 | 35.389 | .52298 | 159.5284 | |
| 2 | 2 | 1 | 51.835 | .38141 | 231.6900 | |
| 0 | 2 | 3 | 60.916 | .94269 | 97.8130 | |

Figure (a) shows powder XRD pattern of $LiMnPO_4$ (2:1) heated at $700^0$C. The XRD is recorded in the 2θ range $10^0$-$80^0$. All the characteristics peaks of $LiMnPO_4$ are present in the investigated diffraction pattern. The sharp and well-resolved diffraction peaks of $LiMnPO_4$ (4:1) confirms crystalline nature of $LiMnPO_4$. The material is formed as single phase.

Table 2: Observed and calculated d-spacing using UNIT CELL software for $LiMnPO_4$ (2:1).

| No | h | k | l | d(obs) Å | d(calc) Å |
|---|---|---|---|---|---|
| 1 | 0 | 2 | 0 | 5.23005 | 5.23002 |
| 2 | 0 | 1 | 1 | 4.32033 | 4.32038 |
| 3 | 1 | 2 | 0 | 3.97036 | 3.97045 |
| 4 | 1 | 1 | 1 | 3.52564 | 3.52565 |
| 5 | 2 | 0 | 0 | 3.04996 | 3.04997 |
| 6 | 0 | 3 | 1 | 2.80948 | 2.80948 |
| 7 | 0 | 4 | 0 | 2.61502 | 2.61501 |
| 8 | 1 | 3 | 1 | 2.55181 | 2.55183 |
| 9 | 2 | 2 | 2 | 1.76283 | 1.76282 |
| 10 | 3 | 3 | 1 | 1.64718 | 1.64718 |

Fig.(b) shows the powder XRD pattern of LiMnPO4 (4:1) heated at $700^0$C. Fig (c): XRD pattern of $LiMnPO_4$ (6:1)

| h | k | l | 2θ (degree) | FWHM | Grain size(nm) | Mean(nm) |
|---|---|---|---|---|---|---|

The XRD is recorded in the 2θ range $10^0$-$80^0$. All the characteristics peaks of $LiMnPO_4$ are present in the investigated diffraction pattern. The sharp and well-resolved diffraction peaks of $LiMnPO_4$ (4:1) confirms crystalline nature of $LiMnPO_4$. The material is formed as single phase.

| No | h | k | l | d (obs) Å | d(calc) Å |
|---|---|---|---|---|---|
| 1 | 0 | 1 | 1 | 4.32035 | 4.32021 |
| 2 | 0 | 2 | 1 | 3.51375 | 3.51373 |
| 3 | 2 | 0 | 0 | 3.04998 | 3.05003 |
| 4 | 0 | 3 | 1 | 2.80949 | 2.80948 |
| 5 | 1 | 3 | 1 | 2.55182 | 2.55184 |
| 6 | 2 | 1 | 1 | 2.49167 | 2.49165 |
| 7 | 2 | 2 | 1 | 2.30331 | 2.30332 |
| 8 | 2 | 2 | 2 | 1.76283 | 1.76279 |
| 9 | 3 | 3 | 1 | 1.64719 | 1.64720 |
| 10 | 0 | 2 | 3 | 1.51355 | 1.51357 |

Table 3: Grain size of $LiMnPO_4$ (4:1) using Scherrer formula

Table 4: Observed and calculated d-spacing using UNIT CELL software for $LiMnPO_4$ (4:1).

| | | | | | | |
|---|---|---|---|---|---|---|
| 0 | 2 | 1 | 25.464 | .47465 | 171.677 | 182.999 |
| 2 | 0 | 0 | 29.431 | .53052 | 154.902 | |
| 1 | 3 | 1 | 35.355 | .37599 | 221.877 | |
| 2 | 2 | 2 | 52.028 | .47145 | 187.599 | |
| 3 | 3 | 1 | 55.913 | .50286 | 178.944 | |

Table 5: Grain size of $LiMnPO_4$ (6:1) using Scherrer formula

The XRD is recorded in the 2θ range $10^0$-$80^0$. All the characteristics peaks of $LiMnPO_4$ are present in the investigated diffraction pattern. The sharp and well-resolved diffraction peaks of $LiMnPO_4$ (6:1) confirms crystalline nature of $LiMnPO_4$.

| h | k | l | 2θ (degree) | FWHM | Grain size (nm) | Mean (nm) |
|---|---|---|---|---|---|---|
| 0 | 2 | 0 | 16.929 | .35736 | 224.221 | 221.355 |
| 0 | 1 | 1 | 20.588 | .34771 | 232.33 | |
| 2 | 0 | 0 | 29.206 | .38479 | 213.458 | |
| 1 | 3 | 1 | 35.529 | .42570 | 196.060 | |
| 2 | 2 | 2 | 51.947 | .36730 | 240.710 | |

| no | h | k | l | d(obs)Å | d(cal)Å |
|---|---|---|---|---|---|
| 1 | 0 | 2 | 0 | 5.23007 | 5.23099 |
| 2 | 0 | 1 | 1 | 4.32035 | 4.31791 |
| 3 | 1 | 2 | 0 | 3.97038 | 3.97096 |
| 4 | 1 | 1 | 1 | 3.52566 | 3.52437 |
| 6 | 0 | 3 | 1 | 2.80949 | 2.80910 |
| 7 | 1 | 3 | 1 | 2.55182 | 2.55157 |
| 8 | 1 | 4 | 0 | 2.40345 | 2.40386 |
| 9 | 1 | 1 | 2 | 2.16023 | 2.16166 |
| 10 | 2 | 2 | 2 | 1.76283 | 1.76219 |
| 11 | 4 | 0 | 0 | 1.52500 | 1.52507 |

Table 6: Observed and calculated d-spacing using UNIT CELL software for $LiMnPO_4$ (6:1).

| h | k | l | 2θ (degree) | FWHM | Grain size(nm) | Mean (nm) |
|---|---|---|---|---|---|---|
| 0 | 1 | 1 | 20.515 | .30645 | 263.580 | |
| 2 | 0 | 0 | 29.255 | .45185 | 181.798 | |

| No | h | k | l | d(obs)Å | d(calc) Å |
|---|---|---|---|---|---|
| 1 | 0 | 2 | 0 | 5.23007 | 5.23243 |
| 2 | 0 | 1 | 1 | 4.32035 | 4.31834 |
| 3 | 1 | 2 | 0 | 3.97038 | 3.97162 |
| 4 | 1 | 0 | 1 | 3.74477 | 3.74333 |
| 5 | 1 | 1 | 1 | 3.52566 | 3.52463 |
| 6 | 2 | 0 | 0 | 3.04998 | 3.05019 |
| 7 | 0 | 3 | 1 | 2.80949 | 2.80966 |
| 8 | 1 | 3 | 1 | 2.55182 | 2.55200 |
| 9 | 2 | 1 | 1 | 2.49167 | 2.49138 |
| 10 | 1 | 1 | 2 | 2.16023 | 2.16181 |
| 11 | 2 | 2 | 2 | 1.76283 | 1.76231 |
| 12 | 1 | 4 | 2 | 1.68826 | 1.68803 |
| 13 | 4 | 0 | 0 | 1.52500 | 1.52509 |

Figure (d) shows the powder XRD pattern of $LiMnPO_4$ (8:1) heated at $700^0$ C. The XRD is recorded in the 2θ range $10^0$-$80^0$.All the characteristics peaks of $LiMnPO_4$ are present in the investigated diffraction pattern. The intense and well-resolved diffraction peaks of $LiMnPO_4$ (8:1) confirms the crystalline nature of $LiMnPO_4$.

Fig (d): XRD pattern of $LiMnPO_4$ (8:1)

Table 7: Grain size of $LiMnPO_4$ (8:1) using Scherrer formula

| | | | | | | |
|---|---|---|---|---|---|---|
| 1 | 3 | 1 | 35.383 | .56811 | 146.853 | 355.224 |
| 1 | 1 | 2 | 41.754 | .35867 | 237.176 | |
| 2 | 2 | 2 | 51.89 | .09335 | 946.712 | |

Table 8: Observed and calculated d-spacing using UNIT CELL software for $LiMnPO_4$ (8:1).

| h | k | l | 2θ (degree) | FWHM | Grain size (nm) | Mean (nm) |
|---|---|---|---|---|---|---|
| 0 | 1 | 1 | 20.628 | .35006 | 230.785 | 317.955 |
| 1 | 1 | 1 | 25.300 | .37102 | 219.550 | |
| 2 | 0 | 0 | 29.200 | .30881 | 265.973 | |
| 1 | 3 | 1 | 35.572 | .54158 | 154.12 | |
| 4 | 0 | 0 | 61.125 | 1.2832 | 719.349 | |

Table 9: Grain size of $LiMnPO_4$ (10:1) using Scherrer formula

Figure (e) shows the powder XRD pattern of $LiMnPO_4$ (10:1) heated at $700^0$C. The XRD is recorded in the 2θ range $10^0$-$80^0$.All the characteristics peaks of LiMnPO4 are present in the investigated diffraction pattern. The sharp intense and well-resolved diffraction peaks of $LiMnPO_4$ (10:1) confirms the crystalline nature of $LiMnPO_4$.

Fig (e): XRD pattern of $LiMnPO_4$ (10:1)

| Unit cell Parameters | Ratio (2:1) | Ratio (4:1) | Ratio (6:1) | Ratio (8:1) | Ratio (10:1) |
|---|---|---|---|---|---|
| a (Å) | 6.09994± 0.00063 | 6.10005± 0.00082 | 6.10027± 0.00041 | 6.10038± 0.00039 | 6.10019± 0.00078 |
| b (Å) | 10.46005± 0.00109 | 10.46039± 0.00182 | 10.46199± 0.00112 | 10.46485± 0.00141 | 10.46002± 0.00195 |
| c (Å) | 4.74394± 0.00067 | 4.74369± 0.00036 | 4.74050± 0.00046 | 4.74080± 0.00045 | 4.74370± 0.00036 |
| Volume ($Å^3$) | 302.6901± 0.0408 | 302.6897± 0.0425 | 302.5435± 0.0380 | 302.6507± 0.0368 | 302.6864± 0.0473 |

Table 10: Unitcell parameters calculated using UNIT CELL software

Olivine structured Lithium manganese phosphate $LiMnPO_4$ is synthesized in the different sucrose to metal molar ratios *ie.* 2:1, 4:1, 6:1, 8:1, 10:1 by hydrothermal method. The formation of $LiMnPO_4$ is confirmed by XRD analysis. All ratios are crystallised in single phase. The d-spacing, lattice parameters, FWHM, grain size are calculated from XRD pattern. It has been observed that the grain size increases with increasing template ratio. While, unit cell parameters are independent of template ratio.

## SYNTHESIS OF $LiMnPO_4$ USING HYDROTHERMAL METHOD

### (2) Glucose as template

$LiMnPO_4$ is prepared by the hydrothermal method. $LiNO_3$, $Mn(NO_3)_2.4H_2O$ and $NH_4H_2PO_4$ were the starting reagents. Metal nitrates were taken in the stoichiometric ratios and it is dissolved in the distilled water using magnetic stirrer for half an hour. To this solution, $NH_4H_2PO_4$ is added after dissolving in distilled water. Glucose is chosen as the template in the reaction to control various morphological parameters.

The balancing equation is shown below:

$$7\ LiNO_3 + 7\ Mn\ (NO_3)_2.4\ H_2O + 7\ NH_4H_2PO_4 \rightarrow 7LiMnPO_4 + 4\ NH_3 + 43\ H_2O + 24\ NO_2$$

In the present study, template to metal ions ratio is varied from 2:1 to 10:1 to study its effect on the morphology.

Thoroughly mixed solution is transferred to 50 ml Teflon- lined stainless- steel autoclave which was heat treated to $120^0$C for 20 hours. After heat treatment, black colour is obtained

which is transferred to crucible and sintered for 6 hours at $700^0$C (fig 1a&b). The sample is grinded to fine powders. The above procedure is repeated for other ratios also.

**(a)** **(b)**

**Fig 1: (a)** Powder sample in crucible before sintering **(b)** sample after sintering

In the present work, 5 samples were characterized by XRD and FTIR techniques. For our convenience and to identify the sample according to their template ratio, let us name them as:

Sample 1 - 2:1

Sample 2 -4:1

Sample 3 -6:1

Sample 4 -8:1

Sample 5 -10:1

**XRD ANALYSIS**

For the structural characterization, XRD was taken for all the powered samples in the 2θ range $10^0$ – $80^0$ at room temperature. The obtained XRD pattern was analyzed using Xpert highscore software. XRD pattern of all the samples were search and matched with the standard database available in the software. From the standard pattern, it is evident that the synthesized samples were crystallized in orthorhombic structure.

The 2θ values of samples were compared with that of standard. From this, d spacing values were selected. Using d spacing and (h k l) values, unit cell software was compiled. The result of the analysis gave the unitcell parameters and volume of unit cell. The same procedure is repeated is for all ratios.

**(A) Sample 1**

The d spacing values and (h k l) values of the sample 1 is tabulated in the table 1 below:

**Table 1:** (h k l) values and comparison of corresponding d values of sample 1

| No: | h | k | l | d(obs) [$A^0$] | d(calc) [$A^0$] | res(d) | 2θ(obs) [deg] | 2θ(calc) [deg] | res (2 θ) |
|---|---|---|---|---|---|---|---|---|---|
| 1 | 0 | 2 | 1 | 3.50347 | 3.51510 | -0.0116 | 25.402 | 25.317 | 0.0852 |
| 2 | 2 | 0 | 0 | 3.05765 | 3.05234 | 0.00530 | 29.183 | 29.235 | -0.052 |
| 3 | 1 | 3 | 1 | 2.54932 | 2.55349 | -0.0042 | 35.175 | 35.115 | 0.059 |
| 4 | 0 | 4 | 1 | 2.29590 | 2.29190 | 0.00400 | 39.207 | 39.278 | -0.071 |
| 5 | 1 | 1 | 2 | 2.16533 | 2.16289 | 0.00243 | 41.678 | 41.727 | -0.049 |
| 6 | 2 | 2 | 2 | 1.76023 | 1.76330 | -0.0031 | 51.903 | 51.806 | 0.097 |

**(B) SAMPLE 2**

The XRD pattern of this sample matches with the standard pattern of $LiMnPO_4$ proving the occurrence of nano structure of lithiophilite and is shown in figure 2. The pattern is shown and the values in comparison are tabulated accordingly in table 2.

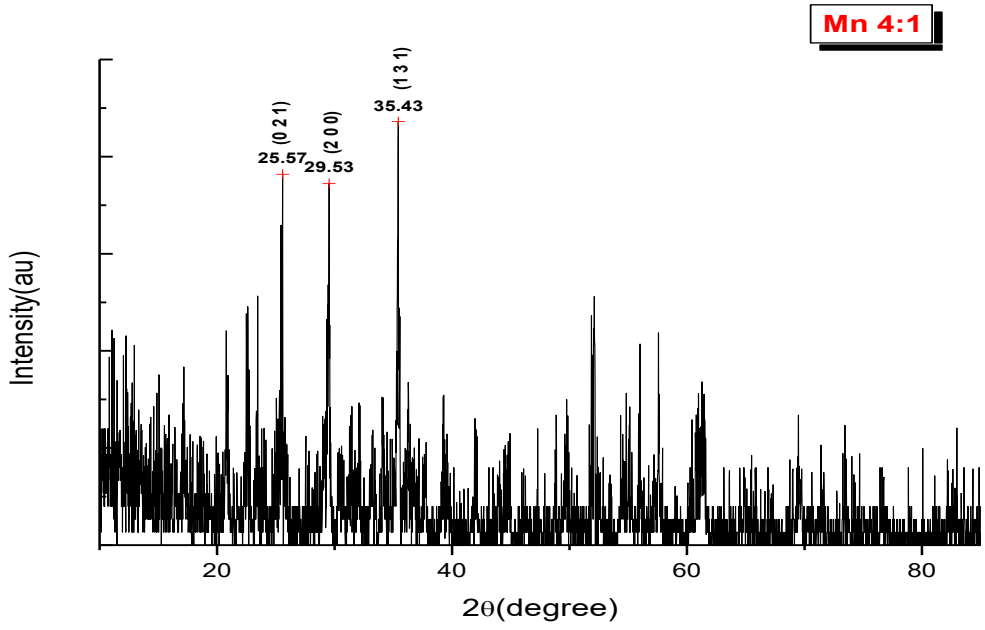


**Fig 2:** XRD pattern of sample 2

The highest intensity peak is obtained at a 2θ value of 35.43 and (h k l) value is (1 3 1).

**Table 2:** (h k l) values and comparison of corresponding d values of sample 2

| No: | h | k | l | d(obs) [$A^0$] | d(calc) [$A^0$] | res(d) | 2θ(obs) [deg] | 2θ(calc) [deg] | res(2θ) |
|---|---|---|---|---|---|---|---|---|---|
| 1 | 0 | 2 | 1 | 3.50040 | 3.51475 | -0.0144 | 25.425 | 25.320 | 0.106 |
| 2 | 2 | 0 | 0 | 3.05304 | 3.05425 | -0.0012 | 29.228 | 29.216 | 0.012 |
| 3 | 1 | 2 | 2 | 2.04248 | 2.03823 | 0.00425 | 44.313 | 44.411 | -0.097 |
| 4 | 1 | 5 | 1 | 1.82742 | 1.82559 | 0.00183 | 49.861 | 49.915 | -0.053 |
| 5 | 1 | 6 | 0 | 1.67666 | 1.67493 | 0.00174 | 54.700 | 54.761 | -0.061 |
| 6 | 1 | 5 | 2 | 1.51600 | 1.51968 | -0.0037 | 61.077 | 60.913 | 0.163 |

The XRD pattern of this sample matches with the standard pattern of $LiMnPO_4$ and is shown in figure 3. The values are tabulated in table 3.

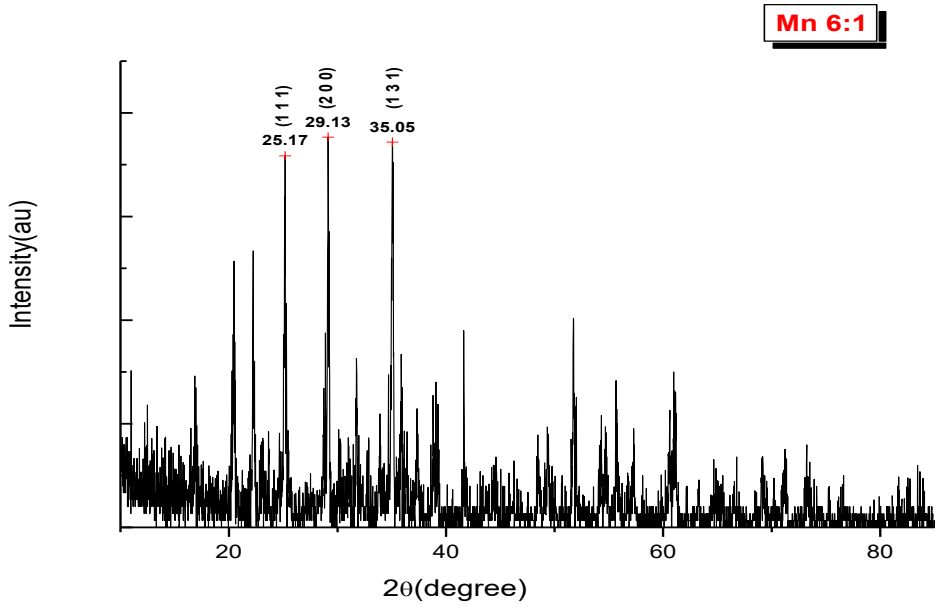


**Fig 3:** XRD pattern of sample 3

The highest intensity peak is obtained at a 2θ value of 35.05 and (h k l) value is (1 3 1).

**Table 3:** (h k l) values and comparison of corresponding d values of sample 3

| No: | h | k | l | d(obs) [$A^0$] | d(calc) [$A^0$] | res(d) | 2θ(obs) [deg] | 2θ(calc) [deg] | res(2θ) |
|---|---|---|---|---|---|---|---|---|---|

| | | | | | | | | | |
|---|---|---|---|---|---|---|---|---|---|
| 1 | 1 | 2 | 0 | 3.98257 | 3.97941 | 0.00316 | 22.305 | 22.323 | -0.018 |
| 2 | 2 | 0 | 0 | 3.08146 | 3.06530 | 0.01616 | 28.953 | 29.108 | -0.156 |
| 3 | 1 | 3 | 1 | 2.54678 | 2.54883 | -0.0021 | 35.211 | 35.182 | 0.029 |
| 4 | 2 | 3 | 1 | 2.05179 | 2.06836 | -0.0166 | 44.102 | 43.730 | 0.371 |
| 5 | 2 | 2 | 2 | 1.76158 | 1.75851 | 0.00307 | 51.861 | 51.958 | -0.097 |
| 6 | 2 | 7 | 1 | 1.29326 | 1.29189 | 0.00137 | 73.114 | 73.204 | -0.090 |

**(D) SAMPLE 4**

The d spacing values and (h k l) values of the sample 4 is tabulated in the table 4 below:

**Table 4:** (h k l) values and comparison of corresponding d values of sample 4

| **No:** | **h** | **k** | **l** | **d(obs) [$A^0$]** | **d(calc) [$A^0$]** | **res(d)** | **2θ(obs) [deg]** | **2θ(calc) [deg]** | **res(2θ)** |
|---|---|---|---|---|---|---|---|---|---|
| 1 | 2 | 1 | 1 | 2.49669 | 2.48987 | 0.00681 | 35.941 | 36.043 | -0.102 |
| 2 | 1 | 5 | 1 | 1.82162 | 1.82158 | 0.00004 | 50.031 | 50.033 | -0.001 |
| 3 | 0 | 6 | 0 | 1.73737 | 1.73869 | -0.0013 | 52.639 | 52.595 | 0.043 |
| 4 | 4 | 0 | 2 | 1.28072 | 1.28199 | -0.0013 | 73.949 | 73.864 | 0.085 |
| 5 | 2 | 4 | 3 | 1.23314 | 1.23294 | 0.00020 | 77.315 | 77.330 | -0.015 |
| 6 | 4 | 6 | 1 | 1.11516 | 1.11474 | 0.00042 | 87.380 | 87.421 | -0.042 |

**(E) SAMPLE 5**

The XRD pattern of this sample matches with the standard pattern of $LiMnPO_4$ and is shown in figure 4. The values are tabulated in table 5.

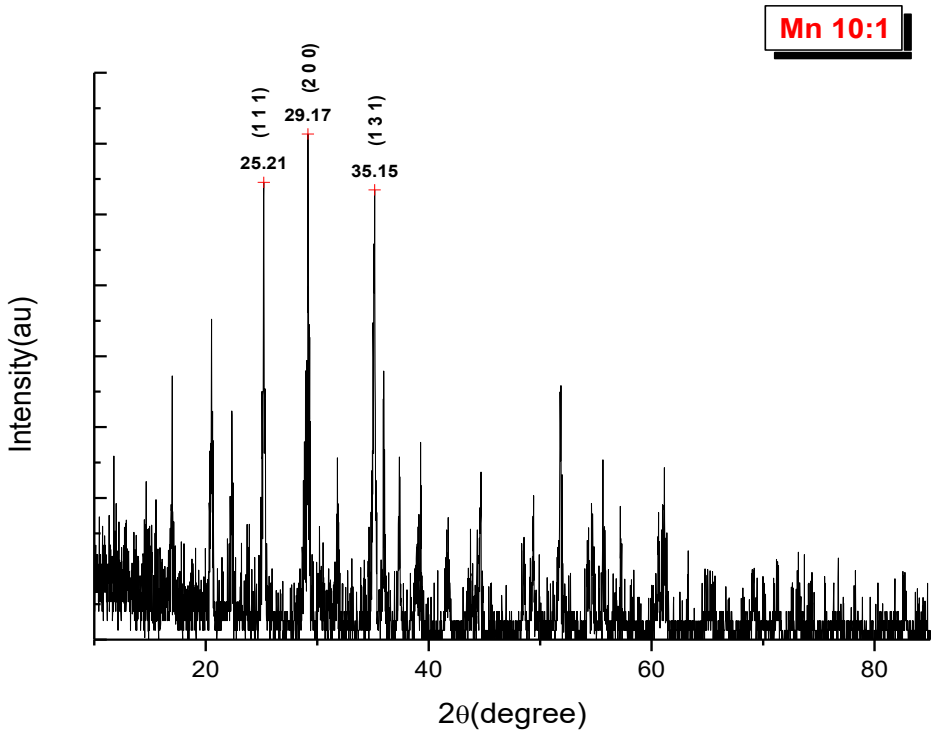


**Fig 4:** XRD pattern of sample 5

The highest intensity peak is obtained at a 2θ value of 35.15 and (h k l) value is (1 3 1).

**Table 5:** (h k l) values and comparison of corresponding d values of sample 5

| **No:** | **h** | **k** | **l** | **d(obs) [$A^0$]** | **d(calc) [$A^0$]** | **res(d)** | **2θ(obs) [deg]** | **2θ(calc) [deg]** | **res(2θ)** |
|---|---|---|---|---|---|---|---|---|---|
| 1 | 0 | 2 | 0 | 5.23575 | 5.26399 | -0.0282 | 16.921 | 16.829 | 0.091 |
| 2 | 1 | 1 | 1 | 3.52933 | 3.52375 | 0.0058 | 25.213 | 25.254 | -0.041 |
| 3 | 2 | 2 | 2 | 1.76658 | 1.76188 | 0.00471 | 51.703 | 51.851 | -0.148 |
| 4 | 3 | 4 | 0 | 1.60581 | 1.60529 | 0.00052 | 57.331 | 57.351 | -0.020 |
| 5 | 0 | 2 | 3 | 1.51518 | 1.51444 | 0.00075 | 61.113 | 61.146 | -0.033 |
| 6 | 2 | 7 | 1 | 1.29721 | 1.29659 | 0.00062 | 72.856 | 72.897 | -0.040 |

The lattice parameters and the volume of unit cell for different samples which were obtained from unitcell software is tabulated in the table 6 below:

**Table 6:** a,b,c values and volume of the unit cell

| SAMPLE | $D_{hkl}$ [$A^0$] |
|---|---|
| Mn 2:1 | 1240.2235 |
| Mn 4:1 | 200.0709 |
| Mn 6:1 | 291.7282 |
| Mn 8:1 | 146.659 |
| Mn 10:1 | 271.7359 |

**FTIR ANALYSIS**

**(A) SAMPLE 1**

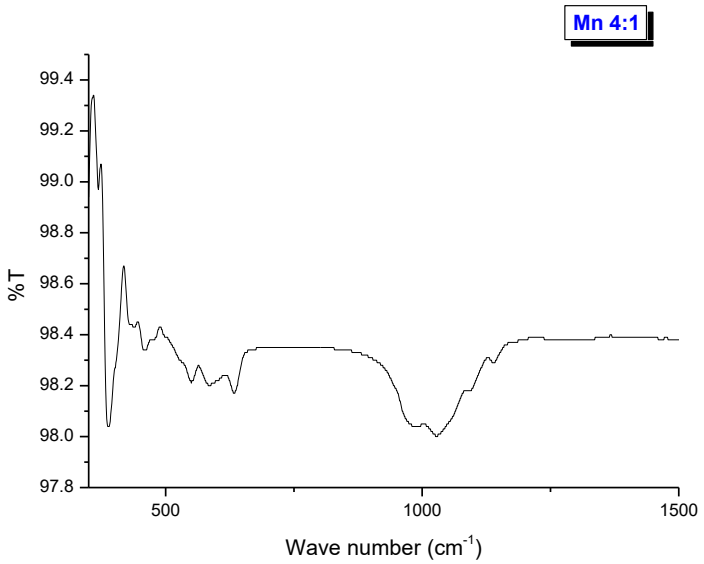


**(C) SAMPLE 3**

| sample | a [$A^0$] | b [$A^0$] | c [$A^0$] | Volume ($10^6$ $pm^3$) |
|---|---|---|---|---|
| Mn 2:1 | 6.1047 | 10.4713 | 4.7430 | 303.1909 |
| Mn 4:1 | 6.1085 | 10.4501 | 4.7500 | 303.2164 |
| Mn 6:1 | 6.1306 | 10.4625 | 4.7087 | 302.0228 |
| Mn 8:1 | 6.1062 | 10.4322 | 4.7226 | 300.8344 |
| Mn10:1 | 6.0771 | 10.5280 | 4.7439 | 303.5094 |

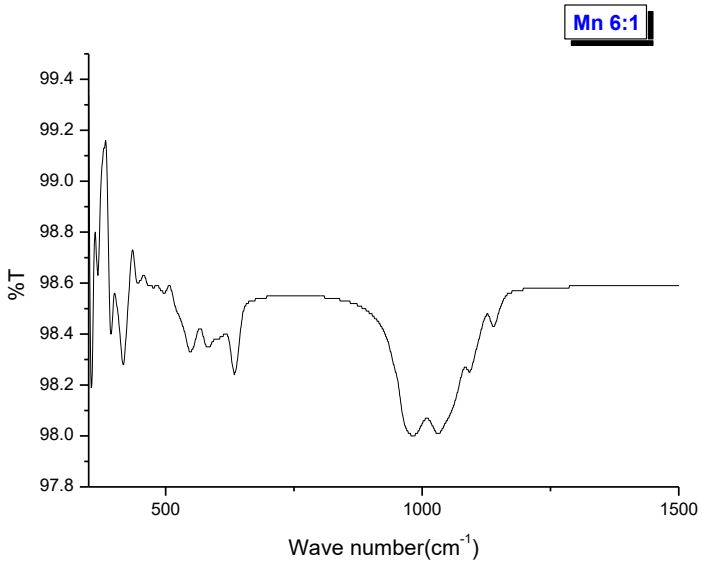


**(C) SAMPLE 4**

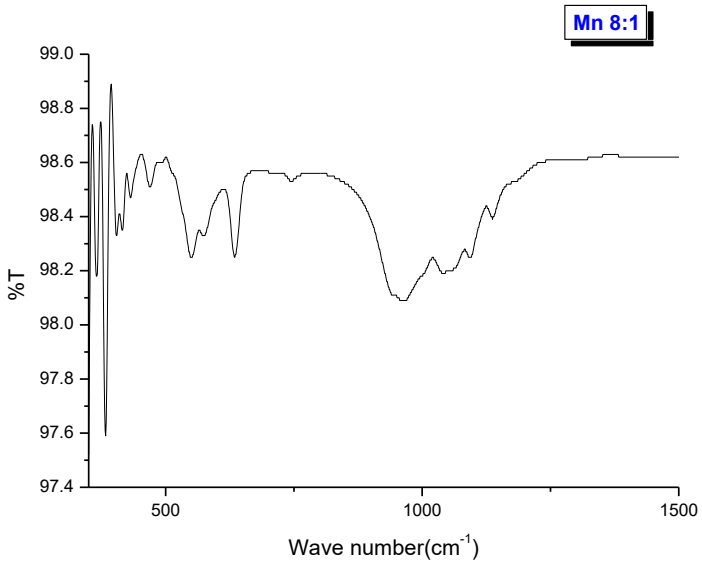


**(D) SAMPLE 5**

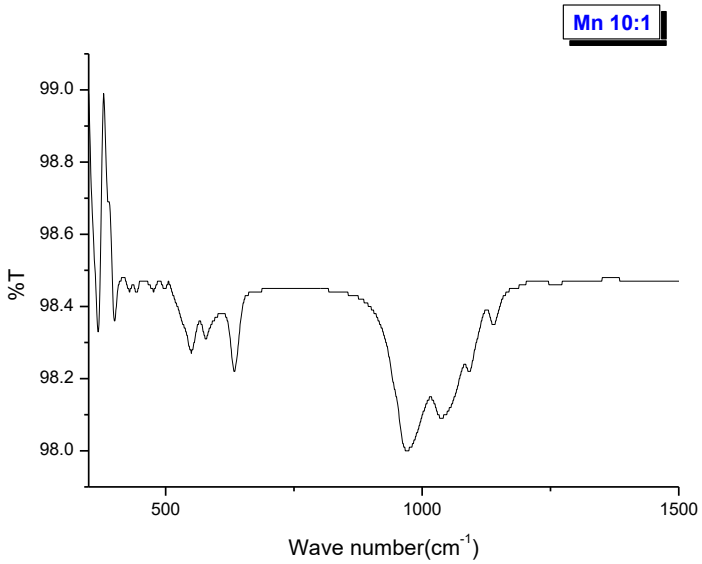


It is a very simple and scalable pathway towards synthesis of metal nitrate hollow spheres. After the hydrothermal treatment of mixtures of carbohydrates with metal salts in water in sealed steel autoclaves at 120 °C, carbon spheres with the metal precursors tightly embedded in the microspheres were obtained. The removal of carbon directly results in hollow spheres of the corresponding metal nitrates that are composed of nanoparticles with high surface areas.

Glucose is used as template in five different molar ratios with metal ions. The synthesized samples are formed as microcrystallites of $LiMnPO_4$ with few impurity peaks. Using UNITCELL software, lattice parameters and cell volume are calculated. Local structure confirmed the formation of $LiMnPO_4$ structure by exploring FTIR studies. Irregularity in the crystallite size and cell parameters might be an indication of failure in the selection of template material. The morphological analysis can be done using electron microscopic analysis.

## (II) SYNTHESIS OF $LiNiPO_4$ USING HYDROTHERMAL METHOD

Hydrothermal process is a technique in which a heterogeneous reaction in the presence of aqueous solvents under high pressure and temperature conditions to dissolve and recrystallize materials that are relatively insoluble under ordinary conditions. Hydrothermal technique is ideal for processing of very fine powders having high purity, controlled stoichiometry, high quality, narrow particle size distribution, a controlled morphology, uniformity, less defects, dense particles, high crystallinity, excellent reproducibility, controlled microstructure, and high reactivity with ease of sintering and so on.

Hydrothermal method is used for the synthesis of $LiNiPO_4$ in nanocrystalline form. $LiNiPO_4$ is prepared from $LiNO_3$, Ni $(NO_3)_2$ $4H_2O$ and $NH_4H_2PO_4$. Chemical reagents and sucrose where mixed in 2:1, 4:1, 6:1, 8:1, 10:1 template: metal ratios in double distilled water and stirred at room temperature. The solution transferred to 50 ml Teflon- limed stainless- steel autoclave was heat treated to $120^0$C for 20 hours; the products obtained were precipitated directly at the bottom of autoclave and calcined. Thus the sample is black in colour ,it is due to the presence of carbon. Reaction is carried out in a sucrose medium which acts as template. For the preparation of $LiNiPO_4$ in 2:1 moles, using sucrose as template, mole percentage of template is 2% and that of metal nitrates is 1%. The obtained sample is finely powdered and sintered for 6 hours at $600^0$C. The sample is grinded to fine powders. Hence we obtain yellow colored sample, due to the removal of carbon at high temperature. Due to the reThe above procedure is repeated for 4:1, 6:1, 8:1, 10:1 template-metal ion ratios. The chemical reaction is given below:

$$7LiNO_3 + 7\ Ni\ (NO_3)_2\ .4\ H_2O + 7\ NH_4H_2PO_4 \rightarrow 7\ LiNiPO_4 + 4\ NH_3 + 43\ H_2O + 24\ NO_2$$

Fig. 3 shows synthesis of metal oxide hollow spheres from hydrothermally treated carbohydrate/metal salt mixtures. During the hydrothermal treatment, carbon spheres are formed with metal ions incorporated into their hydrophilic shell. The removal of carbon via calcination yields hollow metal oxide spheres. Using this process, wide range of metal oxide hollow spheres can be produced that are composed of nanoparticles. The surface area and thickness of the shell can be varied or controlled by the carbohydrate: metal salt concentration. The hollow spheres exhibit diameters from one to several micrometers and consist of nanocrystals of the respective metal oxides. After this, the metal oxide-carbon composites were heated at 600°C for 6h to remove the carbon core, leading to hollow metal oxide particles.

**Schematic Illustration of the Synthesis of Metal Oxide Hollow Spheres from Hydrothermally Treated Carbohydrate/Metal Salt Mixtures**

**Fig:4. The images of sample calcined at $120^0$C and (d) samples calcined at $700^0$C.**

## XRD ANALYSIS

X- ray diffraction is an important tool to determine the crystal structure of materials. X- rays are electromagnetic radiations having shorter wavelength (in the order of 0.1nm). The formation of $LiNiPO_4$ is confirmed by the XRD analysis. The XRD pattern of the samples analysed using Xpert high score software. The graphs are plotted using ORIGIN software. The grain size is calculated from the FWHM of the prominent peaks using Scherrer formula. The d-spacing and lattice parameters are calculated using UNIT CELL software. The grain size is calculated by using Scherrer formula.

## XRD pattern of 2:1 template-metal ratio

**Table 1.1:** Observed and calculated d-spacing using UNITCELL software for $LiNiPO_4$(2:1)

| No. | h | K | l | d (obs) Å | d (cal)Å |
|---|---|---|---|---|---|
| **1** | 0 | 2 | 0 | 5.0926 | 5.2217 |
| **2** | 0 | 1 | 1 | 4.3329 | 4.2775 |
| **3** | 1 | 2 | 0 | 3.8938 | 3.8586 |
| **4** | 1 | 0 | 1 | 3.4754 | 3.6280 |
| **5** | 1 | 2 | 1 | 2.9685 | 2.9794 |
| **6** | 2 | 2 | 0 | 2.4796 | 2.5107 |
| **7** | 1 | 1 | 2 | 2.1261 | 2.1243 |
| **8** | 1 | 2 | 2 | 1.9970 | 2.0036 |
| **9** | 2 | 2 | 2 | 1.7302 | 1.7135 |
| **10** | 3 | 4 | 0 | 1.5475 | 1.5410 |

**Table 1.2:**Unit cell parameters calculated using UNITCELL software

| Lattice parameter | values |
|---|---|
| **a (Å)** | 5.72709±0.00080 |
| **b (Å)** | 10.44340±0.00237 |
| **c (Å)** | 4.68889±0.00039 |

| Cell volume (Å$^3$) | 280.4440±0.0429 |
|---|---|

**Table 1.3:**Grain size of $LiNiPO_4$(2:1) using Scherrer formula

| No. | Sample: template ratio | h | k | l | FWHM | Grain size(nm) | Mean grain size(nm) |
|---|---|---|---|---|---|---|---|
| **1** | **1:2** | 0 | 2 | 0 | 0.35655 | 225.417 | 156.245 |
| **2** | | 0 | 1 | 1 | 0.72605 | 111.168 | |
| **3** | | 1 | 2 | 0 | 0.47154 | 171.909 | |
| **4** | | 1 | 0 | 1 | 0.40506 | 201.159 | |
| **5** | | 1 | 2 | 1 | 0.97460 | 84.370 | |
| **6** | | 2 | 2 | 0 | 0.58250 | 143.449 | |

**XRD pattern of 4:1 template-metal ratio**

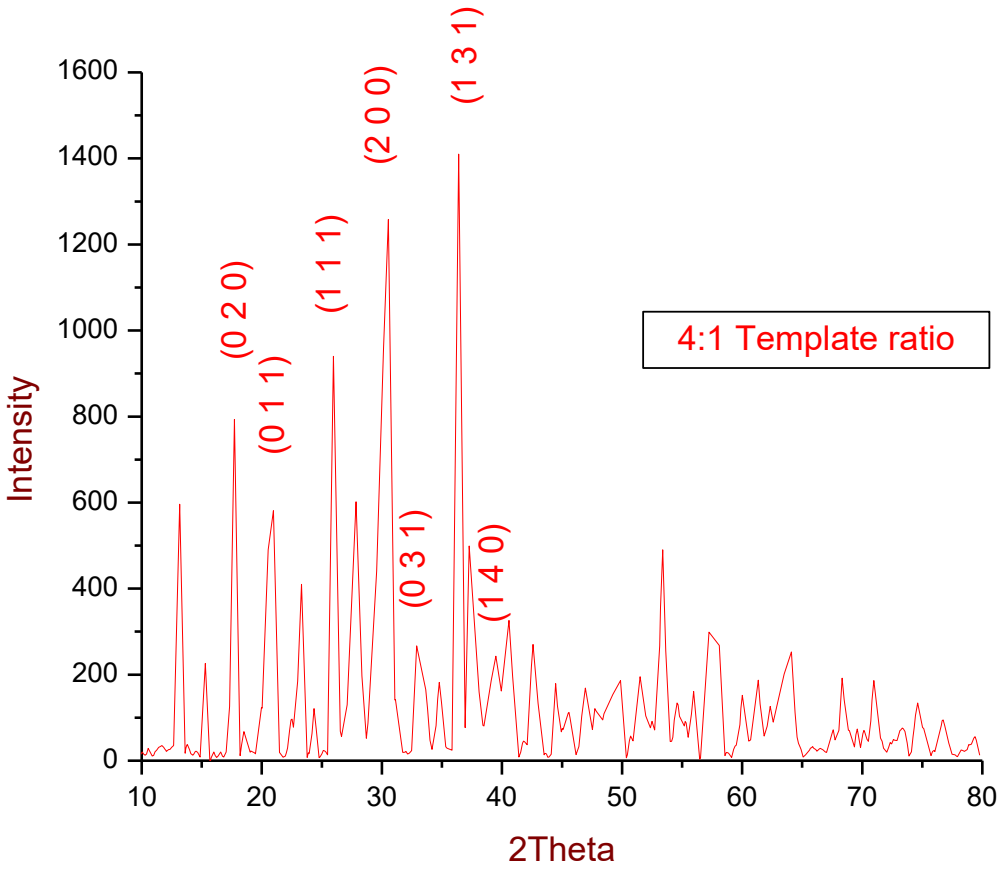


**Table 2.1**: Observed and calculated d-spacing using UNITCELL software for $LiNiPO_4$(4:1)

| No. | h | k | l | d (obs)Å | d (cal)Å |
|---|---|---|---|---|---|
| **1** | 0 | 2 | 0 | 5.0216 | 4.9675 |
| **2** | 0 | 1 | 1 | 4.2703 | 4.2224 |
| **3** | 1 | 1 | 1 | 3.4333 | 3.4311 |
| **4** | 2 | 0 | 0 | 2.9478 | 2.9434 |
| **5** | 0 | 3 | 1 | 2.6996 | 2.7003 |
| **6** | 1 | 3 | 1 | 2.4550 | 2.4544 |
| **7** | 1 | 4 | 0 | 2.2825 | 2.2884 |
| **8** | 2 | 2 | 1 | 2.2248 | 2.2255 |
| **9** | 1 | 1 | 2 | 2.1162 | 2.1184 |
| **10** | 1 | 2 | 2 | 1.9842 | 1.9872 |

**Table 2.2:**Unit cell parameters calculated using UNITCELL software

| Lattice parameter | Values |
|---|---|
| **a (Å)** | 5.88695±0.00076 |
| **b (Å)** | 9.93515±0.00105 |
| **c (Å)** | 4.66464±0.00044 |
| **Volume($Å^3$)** | 272.8239±0.0379 |

**Table 2.3:**Grain size of $LiNiPO_4$(4:1) using Scherrer formula

| No. | Sample: template ratio | h | k | l | FWHM | Grain size(nm) | Mean grain size(nm) |
|---|---|---|---|---|---|---|---|
| **1** | **1:4** | 0 | 2 | 0 | 0.26722 | 300.840 | 317.318 |
| **2** | | 0 | 1 | 1 | 0.50374 | 160.333 | |
| **3** | | 1 | 1 | 1 | 0.11529 | 707.268 | |
| **4** | | 2 | 0 | 0 | 0.52863 | 155.725 | |
| **5** | | 1 | 3 | 1 | 0.17473 | 478.750 | |
| **6** | | 1 | 4 | 0 | 0.83569 | 100.997 | |

**3.XRD pattern of 6:1 template ratio**

**Table 3.1:** Observed and calculated d-spacing using UNITCELL software for $LiNiPO_4$(6:1)

| No. | h | k | l | d (obs)Å | d (cal)Å |
|---|---|---|---|---|---|

| | | | | | |
|---|---|---|---|---|---|
| **1** | 0 | 2 | 0 | 4.9983 | 4.9914 |
| **2** | 0 | 1 | 1 | 4.2537 | 4.2410 |
| **3** | 1 | 2 | 0 | 3.8206 | 3.8343 |
| **4** | 1 | 1 | 1 | 3.4301 | 3.4611 |
| **5** | 1 | 2 | 1 | 2.9369 | 2.9672 |
| **6** | 0 | 3 | 1 | 2.7027 | 2.7129 |
| **7** | 1 | 3 | 1 | 2.4588 | 2.4711 |
| **8** | 1 | 1 | 2 | 2.1143 | 2.1312 |
| **9** | 1 | 2 | 2 | 2.0266 | 1.9989 |
| **10** | 2 | 4 | 0 | 1.9265 | 1.9171 |

**Table 3.2:**Unit cell parameters calculated using UNITCELL software

| Lattice parameter | values |
|---|---|
| **a (Å)** | 5.98895±0.00171 |
| **b (Å)** | 9.98282±0.00151 |
| **c (Å)** | 4.68488±0.00044 |
| **Volume ($Å^3$)** | 280.0929±0.0536 |

**Table 3.3:** Grain size of $LiNiPO_4$(6:1) using Scherrer formula

| No | Sample: template ratio | h | k | l | FWHM | Grain size(nm) | Mean grain size(nm) |
|---|---|---|---|---|---|---|---|
| **1** | **1:6** | 0 | 2 | 0 | 0.61968 | 129.762 | 121.287 |
| **2** | | 0 | 1 | 1 | 0.87156 | 92.651 | |
| **3** | | 1 | 2 | 0 | 0.54337 | 149.242 | |
| **4** | | 1 | 1 | 1 | 0.61601 | 132.841 | |
| **5** | | 1 | 2 | 1 | 0.93491 | 88.040 | |
| **6** | | 1 | 3 | 1 | 0.61884 | 135.186 | |

**XRD pattern of 8:1 template ratio**

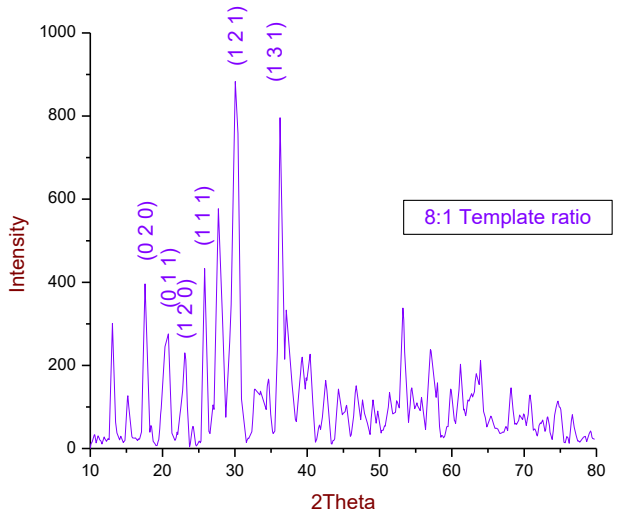


**Table 4.1:** Observed and calculated d-spacing using UNITCELL software for $LiNiPO_4$(8:1)

| No. | h | k | l | d (obs)Å | d (cal)Å |
|---|---|---|---|---|---|
| **1** | 0 | 2 | 0 | 5.0343 | 5.0493 |
| **2** | 0 | 1 | 1 | 4.3289 | 4.2360 |
| **3** | 1 | 2 | 0 | 3.8422 | 3.8373 |
| **4** | 1 | 1 | 1 | 3.4545 | 3.4417 |
| **5** | 1 | 2 | 1 | 2.9534 | 2.9638 |
| **6** | 0 | 3 | 1 | 2.7101 | 2.7300 |
| **7** | 1 | 3 | 1 | 2.4710 | 2.4779 |
| **8** | 2 | 2 | 1 | 2.2225 | 2.2365 |
| **9** | 1 | 1 | 2 | 2.1195 | 2.1214 |
| **10** | 2 | 4 | 0 | 1.9313 | 1.9186 |

**Table 4.2:**Unit cell parameters calculated using UNITCELL software

| Lattice parameter | values |
|---|---|
| **a (Å)** | 5.90379±0.00111 |
| **b (Å)** | 10.09877±0.00137 |
| **c (Å)** | 4.66637±0.00053 |
| **Volume ($Å^3$)** | 278.2140±0.0405 |

**Table 4.3:** Grain size of $LiNiPO_4$(8:1) using Scherrer formula

| No | Sample: template ratio | h | k | l | FWHM | Grain size(nm) | Mean grain size(nm) |
|---|---|---|---|---|---|---|---|
| **1** | **1:8** | 0 | 2 | 0 | 0.16563 | 485.404 | 199.347 |
| **2** | | 0 | 1 | 1 | 0.88438 | 91.288 | |
| **3** | | 1 | 2 | 0 | 0.61639 | 131.531 | |
| **4** | | 1 | 1 | 1 | 0.38327 | 213.596 | |
| **5** | | 1 | 2 | 1 | 0.88766 | 92.675 | |
| **6** | | 1 | 3 | 1 | 0.46050 | 181.589 | |

**XRD pattern of 10:1 template ratio**

**Table 5.1:** Observed and calculated d-spacing using UNITCELL software for $LiNiPO_4$(10:1)

| No. | h | k | L | d (obs)Å | d (cal)Å |
|---|---|---|---|---|---|
| **1** | 0 | 2 | 0 | 4.9390 | 4.9755 |
| **2** | 0 | 1 | 1 | 4.2244 | 4.2209 |
| **3** | 1 | 2 | 0 | 3.8184 | 3.7990 |
| **4** | 1 | 1 | 1 | 3.4024 | 3.4295 |
| **5** | 2 | 0 | 0 | 2.9218 | 2.9415 |
| **6** | 0 | 3 | 1 | 2.6767 | 2.7025 |
| **7** | 1 | 3 | 1 | 2.4375 | 2.4558 |
| **8** | 1 | 1 | 2 | 2.1027 | 2.1170 |
| **9** | 1 | 2 | 2 | 2.0112 | 1.9865 |
| **10** | 2 | 4 | 0 | 1.9131 | 1.8995 |

**Table 5.2:**Unit cell parameters calculated using UNITCELL software

| Lattice parameter | Values |
|---|---|
| a (Å) | 5.88318±0.00082 |
| b (Å) | 9.95110±0.00119 |
| c(Å) | 4.66096±0.00043 |
| Volume ($Å^3$) | 272.8719±0.0379 |

**Table 5.3:**Grain size of $LiNiPO_4$(10:1) using Scherrer formula

| No | Sample: template ratio | h | k | l | FWHM | Grain size(nm) | Mean grain size(nm) |
|---|---|---|---|---|---|---|---|
| 1 | 1:10 | 0 | 2 | 0 | 0.25473 | 315.693 | 205.685 |
| 2 | | 0 | 1 | 1 | 0.58828 | 137.337 | |
| 3 | | 1 | 2 | 0 | 0.44664 | 181.676 | |
| 4 | | 1 | 1 | 1 | 0.28153 | 289.777 | |
| 5 | | 2 | 0 | 0 | 0.88439 | 93.123 | |
| 6 | | 1 | 3 | 1 | 0.38694 | 216.508 | |

Olivine structured $LiNiPO_4$ is synthesized using hydrothermal method for 2:1, 4:1, 6:1, 8:1, 10:1 template-metal ratios. The formation of $LiNiPO_4$ is confirmed by X Ray Diffraction analysis. From the XRD pattern, the values of d-spacing, lattice parameters, FWHM and grain size are calculated. It has been observed that the grain size increases with increasing template ratios. The deviation for 2:1 and 4:1 ratios are due to the variation in sintering process. It has also been observed that the unit cell parameters are independent of template ratios.

The equivalent circuit representation of $LiNiPO_4$ is $R_c(R_gQ_g)(R_{gb}Q_{gb})(Q_eC_e)$, where, $R_c$ is the contact resistance, $R_g$ is the grain resistance and $R_{gb}$ is the grain-boundary resistance. The $Q_g$ and $Q_{gb}$ represent the constant phase element which that is used to explain the depressed semi-circles in the complex impedance representation. The $LiNiPO_4$ synthesized by solution combustion technique shows higher conductivity compared to the microcrystalline material. Its grain dc conductivity is $(1.35\pm0.18)x10^{-6}Scm^{-1}$ at 403K and this value is few orders of magnitude higher than the microcrystalline analogue [39]. The grain and grain-boundary conductivity values are extracted using Boukamp equivalent circuit analysis. The dc conductivity values follow the Arrhenius behaviour. The activation energy, (0.20±0.02)eV of $LiNiPO_4$, is less compared to the

reported value of 0.6eV for microcrystalline materials. The nanocrystalline nature of the material may be the reason for the enhancement in conductivity.

**Vibrating Sample Magnetometer**

The VSM works on Faraday's law, which states that an emf, V, is generated in a coil when there is a change in the magnetic flux linking the coil. For a coil with n turns of area, a, and magnetic flux density, B, the emf generated in the coil is:

$$V=-na\frac{dB}{dt}$$

If the coil is positioned in a constant magnetic field, H, the magnetic flux density in the coil is given by:

$$B=\mu_0 H$$

Consider a sample having magnetization, M, is introduced into the coil then, total magnetic flux in the system is:

$$B=\mu_0(H+M)$$

and the corresponding flux change is:

$$\Delta B=\mu_0 M$$

Combining the Eqs. (2.28) and (2.31) leads to:

$$Vdt=-na\mu_0 M$$

This means that the output signal of the coil is proportional to the magnetization,M, but is independent of the magnetic field in which the size of M is to be determined.

Schematic of vibrating sample magnetometer

The schematic of VSM is shown in Fig.. In the instrument, sample is subjected to a sinusoidal motion; corresponding voltage is induced in suitably located stationary pickup coils. Output signals of these coils have the same frequency and its intensity is proportional to the magnetic moment of the sample, the vibration amplitude and frequency. The sample to be measured is centered in the region between poles of the magnet, able to generate the measurable field $H_0$. A thin vertical sample rod connects the sample holder with a transducer assembly located above the magnet. The transducers convert the sinusoidal ac driven signal into a sinusoidal vertical vibration of the sample rod. Thus, the sample is subjected to sinusoidal vibration in the uniform magnetic field, $H_0$. The coils in the poles of the magnet pick up the signal resulting from the vibration of the sample. This ac signal at the vibration frequency, $\nu$, is proportional to the magnitude of the moment of the sample. However, since it is also proportional to the vibration amplitude and frequency, the moment readings taken simply by measuring the amplitude of the signal are subject to errors due to variations in the amplitude and frequency vibration. In order to avoid these errors, a vibration capacitor for generating reference signal that varies with moment, vibration amplitude and vibration frequency is used in the same manner as the signal from the pickup coils . When these two signals are processed in appropriate way it is possible to eliminate the effects of vibration amplitude and the frequency shifts. In this case obtained readings vary only with the sample moment. Lake Shore Model: 7404 VSM of vibration frequency 82.5Hz and a maximum magnetic field of 15KGauss are used in the present study. The magnetic moment range of the instrument is 1μemu to 56emu.

Qualitative confirmation of electronic contribution of transition metals, like Fe, Cr and Ni, to the electrical conductivity is carried out by room temperature VSM studies. Electronic

contribution to the total conducivity is related to the co-existence of different electronic states. Generally, exchange interaction between equal valence ions is antiferromagnetic and interaction between ions with different valence states like $Fe^{3+}$ ($3d^5$) and $Fe^{2+}$ ($3d^6$) is ferromagnetic.

For olivine type materials, the behaviour of magnetic field is linear with the appearance of small hysteresis loop. These figures show magnified portion of the hystersis loop of $LiNiPO_4$ with small area under the loop. Its overall behaviour is of antiferromagnetic character, with significant difference in the magnetic behaviour. This difference is due to the co-existance of competing antiferromagnetic and ferromagnetic interactions. The ferromagnetic interactions are due to the existence of multiple valency in the material. But, as shown in Fig., the strength of magnetization is very small, approximately 0.28emu/g in the strong magnetic field of 1.2T. These ferromagnetic interactions are weak to contribute for the electronic conductivity in the investigated olivine materials.

**REFERENCES**

1. B.Viswanathan-Nano Materials 5.14-5.16, 9.7

2. Jun Liu, Wen Li and Arumugam Mandiram-chem.commun., 46,**2010**, 1437-1439
3. Yondge Meng,Dairong Chen, and Xiulingjiao- *Eur. J. Inorg. Chem.* **2008** 4019–4023,
4. Maria-magdalenaTitirici, Markus Antonietti, and ArnenThomas- chem. *Mater., Vol. 18, No. 16, **2006**, 3808-3812*
5. Azlinsanusi, Shanti Navaratnam, Wan Jeffrey Basirun- vol 18, **2014**, 522-526
6. K.Zaghib,A.Mauger,F.Gendron, C.M. Julien-O.Garcia-Moreno, M.Alvarez-Vega, F.Garcia-Alvarado, J. Garcia-Jaca, J.M. Gallardo-amores, M.L.Sanjuan and U.Amador-Chem.Mater.**2001**,1570-1576
7. K.Rissouli, K.Benkhouja, J.R.Ramos-Barrado,C.Julien-Materials Science and Engineering, **2003**, 185-189
8. Craig.A.J.Fisher, Veluz M.Hart Prieto, and M.Saiful islam.Chem.Mater, vol.20, **2008**, 5907-5915
9. C.V.Ramana, A.Ait-Salah, S.Utmsunomia, U.Becker, A.Mauger, F.Gendron and C.M.Julien-chem.Mater**, 2006**,3788-379

**iii. Has the progress been according to original plan of work and towards achieving the objective. if not, state reasons.**

Yes the progress been according to original plan of work and towards achieving the objective.

**iv. Please enclose a summary of the findings of the study**

PI has explored hydrothermal method to synthesise various OLINIVE structured using different templates in various ratios. Olivine structured Lithium manganese phosphate $LiMnPO_4$ is synthesized in the different sucrose to metal molar ratios *ie.* 2:1, 4:1, 6:1, 8:1, 10:1 by hydrothermal method. The formation of $LiMnPO_4$ is confirmed by XRD analysis. All ratios are crystallised in single phase. The d-spacing, lattice parameters, FWHM, grain size are calculated from XRD pattern. It has been observed that the grain size increases with increasing template ratio. While, unit cell parameters are independent of template ratio. It is a very simple and scalable pathway towards synthesis of metal nitrate hollow spheres. After the hydrothermal treatment of mixtures of carbohydrates with metal salts in water in sealed steel autoclaves at 120 °C, carbon spheres with the metal precursors tightly embedded in the microspheres were obtained. The removal of carbon directly results in hollow spheres of the corresponding metal nitrates that are composed of nanoparticles with high surface areas.

Glucose is used as template in five different molar ratios with metal ions to synthesise $LiMnPO_4$. The synthesized samples are formed as microcrystallites of $LiMnPO_4$ with few impurity peaks. Using UNITCELL software, lattice parameters and cell volume are calculated. Local structure confirmed the formation of $LiMnPO_4$ structure by exploring FTIR studies. Irregularity in the crystallite size and cell parameters might be an indication of failure in the selection of template material. Irregularity in the crystallite size and cell parameters might be an indication of failure in the selection of template material. The morphological analysis can be done using electron microscopic analysis.It is a very simple and scalable pathway towards synthesis of metal nitrate hollow spheres. After the hydrothermal treatment of mixtures of carbohydrates with metal salts in water in sealed steel autoclaves at 120 °C, carbon spheres with the metal precursors tightly embedded in the microspheres were obtained. The removal of carbon directly results in hollow spheres of the corresponding metal nitrates that are composed of nanoparticles with high surface areas.

Olivine structured $LiNiPO_4$ is synthesized using hydrothermal method for 2:1, 4:1, 6:1, 8:1, 10:1 template-metal ratios. The formation of $LiNiPO_4$ is confirmed by X Ray Diffraction analysis. From the XRD pattern, the values of d-spacing, lattice parameters, FWHM and grain size are calculated. It has been observed that the grain size increases with increasing template ratios. The deviation for 2:1 and 4:1 ratios are due to the variation in sintering process. It has also been observed that the unit cell parameters are independent of template ratios.

PI has produced interesting combination of the OLIVINE for the applications in Li ion batteries. These materials needs to be investigated further to understand the increase in ion conductivity and ion dynamics both microcrystalline and nanocrystalline form.

**v. Any other information**

As mentioned in the objective, electrical and magnetic studies of the synthesised materials are achieved. Since the amount allotted of equipment is not adequate for the purchase of instruments for electrical and magnetic studies. These facilities are availed from other instititions using the fund of contigency and special needs. Electrochemical study is expensive for the budent allotted for the project and hence can't be carried out.